# Microthermal analysis of polymeric materials

Vladimir V. Tsukruk[a,*], Valeriy V. Gorbunov[a,b], Nobi Fuchigami[a,c]

[a]*Department of Materials Science and Engineering, Iowa State University, 3053 Gilman Hall, Ames, IA 50011, USA*
[b]*TM Microscopes, Sunnyvale, CA, USA*
[c]*Angstrom Systems, San Jose, CA, USA*

## Abstract

The technique of scanning thermal microscopy (SThM) with microthermal analysis (μTA) was used for examining the surface thermal properties of a wide selection of materials ranging from poorly thermal conducting polymers to highly conductive metals. We discuss μTA results in comparison with the data collected from conventional methods of thermal analyses, namely, differential scanning calorimetry (DSC) and thermomechanical analysis (TMA). The μTA measurements of melting and glass transition temperatures were conducted using a wide range of heating rates. We demonstrated that the trends observed were consistent with concurrent measurements by DSC. From the comparison of the μTA and TMA results, we concluded that the thermomechanical contribution, which is due to a variable physical contact area for a ''sinking'' tip, was dominant in the microthermal response of polymers.
© 2002 Elsevier Science B.V. All rights reserved.

## 1. Introduction

Since the first publications about scanning thermal microscopy (SThM) and micro-thermal analysis (μTA) [1–3], developments in this area have resulted in many interesting results. The μTA ability to probe surface microthermal properties with a submicron spatial resolution is distinct for surface characterization techniques. This ability has been demonstrated for polymer composites as well as for semiconductor and metal surfaces [1,3–9]. Phase transformations such as the glass transition and melting were detected for various polymers [10,11]. However, to date, this method has not become a universal thermo-analytical tool. There are some issues associated with comprehensive understanding of the results and how they can be compared with conventional thermal analysis methods like differential scanning calorimetry (DSC) and thermomechanical analysis (TMA). The quantitative characterization of surface thermal properties requires non-trivial efforts in the selection of optimal probing conditions and careful data interpretation [6–9,12].

In the present communication, we describe our recent progress on quantitative microprobing of the surface microthermal properties of various materials. We analyze the contribution of the variable physical contact area to the thermal and mechanical signal responses during the loading of the thermal probe. Finally, we compare instrumentation-dependent data acquisition behavior of the μTA technique with the conventional techniques of DSC and TMA.

---

* Corresponding author. Tel.: +1-515-294-6904;
fax: +1-515-294-5444.
*E-mail address:* vladimir@iastate.edu (V.V. Tsukruk).

## 2. Experimental

The SThM approach is based upon the scanning probe microscopy (SPM) principles of the optical detection of the vertical deflection of a cantilever via a laser reflection scheme (Fig. 1). In the μTA method, a thermal probe with an attached ''mirror'' for laser deflection takes the place of the cantilever/tip scheme inherent of SPM. With this approach, an electric bridge is used to keep a constant, pre-determined probe temperature or voltage in addition to the optical detection scheme. The thermal probe is a Wollaston microwire etched at the very end to form a sensing loop with an effective radius of curvature of about 5 μm [3]. This scheme allows for concurrent measurements of the deflection of the cantilever (SPM mode), as well as the heat dissipation of the thermal probe (SThM mode) (Fig. 1). SThM mode is primarily used for the analysis of the heat dissipation of the thermal probe as discussed in detail in several recent publications [3–10]. The heat dissipation, $Q$, is directly related to the parameters of the electric circuit (Fig. 1) as:

$$Q = \frac{V_P^2}{R_P} = V_b^2 \frac{R_P}{(R_P + R_1 + R_L)^2}, \quad \text{(W)} \tag{1}$$
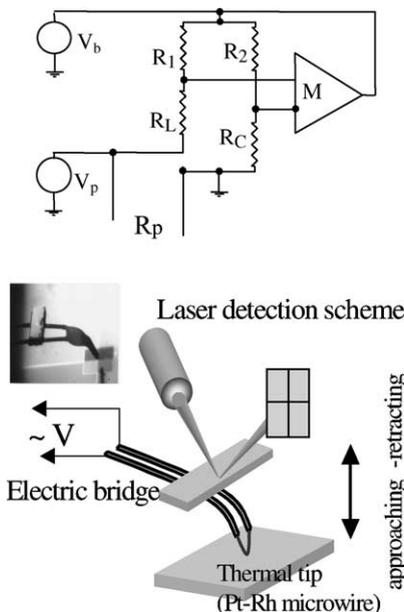


Fig. 1. SThM detection scheme with optical detection of tip deflection and optical image of actual thermal tip (bottom) and electrical bridge detection of heat dissipation (top).

Parameters presented here can be experimentally evaluated and determined from the controller software (Thermomicroscopes Co.).

From the thermal signal–distance data (Fig. 2), one can estimate the surface temperature variation from [8]:

$$T_0 + \delta T(t) \approx T_P - \frac{R_P V_b^2(t)}{(R_P + R_1 + R_L)^2} \frac{Z_0 - vt}{\lambda_{air} \pi r^2}, \quad \text{(K)} \tag{2}$$

where $T_P$ is the probe temperature, $T_0$ the initial surface temperature (room temperature), $Z_0$ the initial distance between the thermal probe and the surface, $v$ the probe approaching velocity, $t$ the probing time, $\lambda_{air}$ the thermal conductivity of air, $r \approx (R_1 \times R_2)^{1/2}$ is the effective radius of the thermal probe, where $R_1$ is the radius of the sensing loop and $R_2$ the radius of the microwire. Eqs. (1) and (2) provide basic relationships between the heat dissipation at the contact point, the surface temperature, the measured experimental data, and instrumentation parameters (for detail discussion see [7–9]).

The samples for microthermal analysis were selected to represent materials with a wide range of surface thermal properties (Table 1). All SThM measurements were conducted using an Explorer microscope with the capability for μTA analysis (Thermomicroscopes Co.). For μTA, we used two

Table 1
Thermal properties of materials (thermal conductivity and thermal diffusivity data as taken from Internet databases of MatWeb, MEMS materials database, CenBASF/materials)

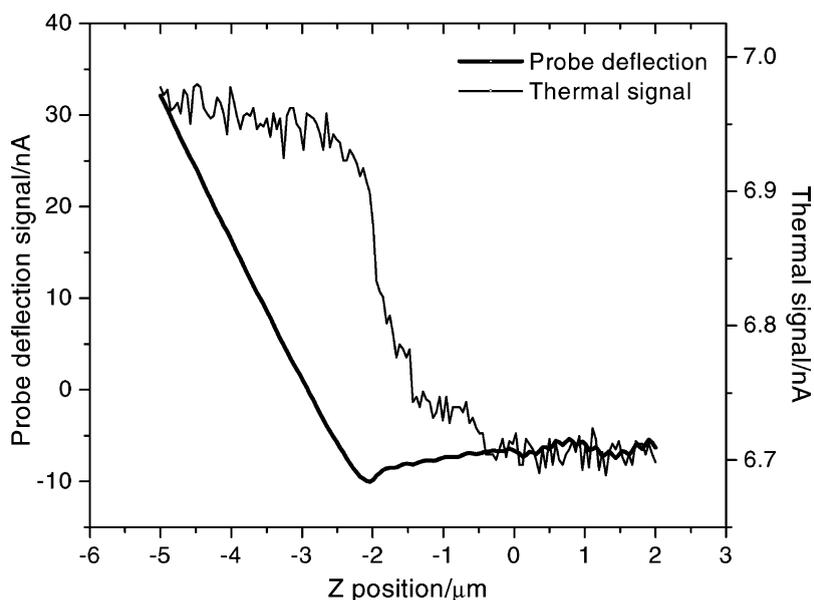| Materials | $\lambda$ (W m$^{-1}$ K$^{-1}$) | $a$ (10$^{-8}$ m$^2$ s$^{-1}$) |
|---|---|---|
| Polystyrene (PS) | 0.142 | 7.52 |
| Polyurethane (PU) | 0.147 | 8.91 |
| Polypropylene (PP) | 0.18 | 9.47 |
| Poly(methyl methacrylate) (PMMA) | 0.19 | 11.77 |
| Poly(vinyl chloride) (PVC) | 0.21 | 14.93 |
| Polyethylene (PEHD) | 0.37 | 17.52 |
| Glass | 1.6 | 67.34 |
| Silicon nitride | 19.0 | 863.24 |
| Graphite | 24.0 | 1543.66 |
| Platinum | 71.0 | 2507.59 |
| Silicon | 156.0 | 9394.33 |
| Gold | 317.0 | 12830.60 |
| Air | 0.024 | 18.4 |

Fig. 2. Thermal signal and cantilever deflection vs. tip/surface distance during the approaching cycle for a polyethylene sample. The approaching velocity is 5 μm s$^{-1}$ and the initial probe temperature is 50 °C.

Pt:Rd (90:10%) thermal probe sensors with one being used as the reference standard [10,13]. Experimental routines are described in detail elsewhere [11]. Conventional DSC and TMA measurements were performed with a Perkins-Elmer Pyris 1 instrument.

## 3. Results and discussion

The approaching–retracting mode was used to collect the force–distance data concurrently with the thermal signal, which is the current measured through the thermal probe. Force–distance data gathering begins several micrometers above the surface (Fig. 2). Force–distance data were used to define the precise point of physical contact between the thermal probe and the surface. We collected thermal data for each material in the range of 35–80 °C.

Using the Block [14] and Jaeger [15] theories, we presented the relationship between the heat dissipation through the contact area during physical contact, $\Delta Q$, for the quasi-steady process in the form [8,9]:

$$\Delta Q = \tfrac{3}{4}\pi\lambda R_C \Delta T, \quad (\text{W}) \tag{3}$$

Here, $\Delta T$ is the initial temperature difference between the probe and the surface, $R_C$ the effective contact radius of the thermal probe, and $\lambda$ the "composite" thermal conductivity, defined as:

$$\frac{2}{\lambda} = \frac{1}{\lambda_S} + \frac{1}{\lambda_P} \tag{4}$$

where $\lambda_P$ and $\lambda_S$ are thermal conductivities for the thermal probe and the surface, respectively [16,17].

Eq. (3) shows that the ratio $\Delta Q/\Delta T \sim \lambda R_C$ should be constant for a given material if the contact radius and the thermal conductivity are unchanged. Fig. 3 presents the measurements of the ratio for selected materials with different thermal and mechanical properties. These results demonstrate that, indeed, this ratio is constant within the interval of probing temperatures used.

Eq. (3) can be represented in different form:

$$\frac{\Delta Q}{\Delta T} = \frac{3}{4}\left(\frac{\lambda_P\pi R_C}{1 - (\lambda_P/\lambda_S)}\right) \tag{5}$$

The contact radius for materials with different Young's modulus was evaluated using Hertzian approximation [18–22]. The results from the analysis of experimental data for all materials listed in Table 1 in terms of Eq. (5) are presented in Fig. 4. Each point on this plot represents the average value for the given surface obtained at several (3–5) locations and 3–4 different
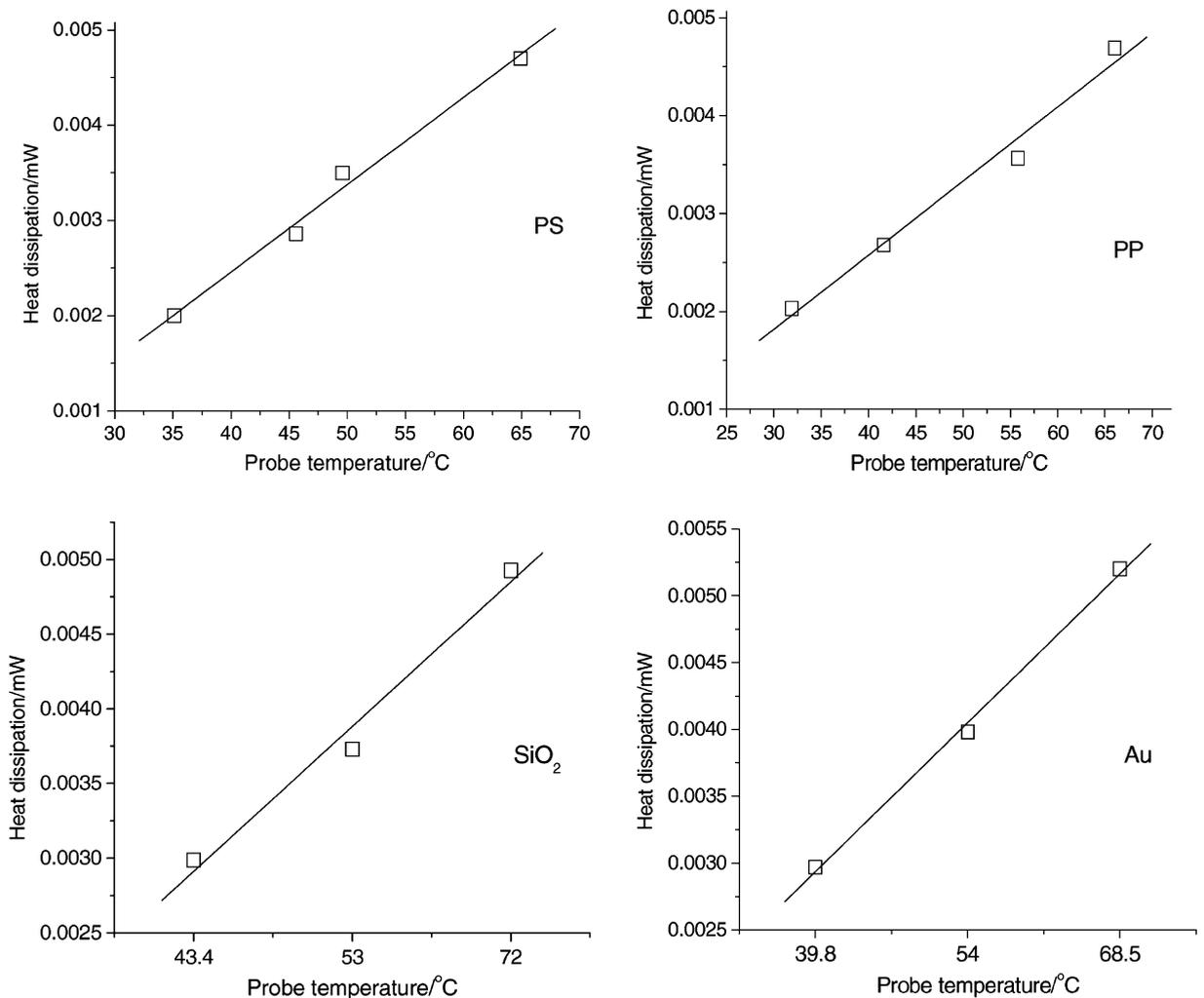
Fig. 3. The variation of the probe heat dissipation vs. initial probe temperature for selected representatives of poorly and highly thermally conductive surfaces (polystyrene and polypropylene vs. glass and gold, respectively), along with their linear approximations.

probe temperatures. We concluded in our previous publications [8,9] that the data could be described fairly well by a linear function. However, we noted that if all the materials studied are grouped separately according to whether the material possesses high or low thermal conductivity, a non-linear behavior becomes evident (Fig. 4).

Indeed, as can be seen in Fig. 4, materials with thermal conductivity below platinum behaved very differently as compared to highly thermal conductive materials. A significant increase in heat dissipation was observed for the first group. In contrast, for

materials with thermal conductivity higher than platinum (two specimens, silicon and gold), only a small increase of $\Delta Q/\Delta T$ was observed. This difference can be understood considering the nature of "composite" thermal conductivity, $\lambda$, for the tip/surface entity, as presented by Eq. (4). This relationship demonstrates that for all surfaces with $\lambda_S \ll \lambda_P$ (polymers, glass, and semiconductors), the "composite" thermal conductivity for the tip/surface entity is primarily determined by the more poorly conductive faction of this entity, namely, the surface. Therefore, under these conditions, the "composite" thermal conductivity that is
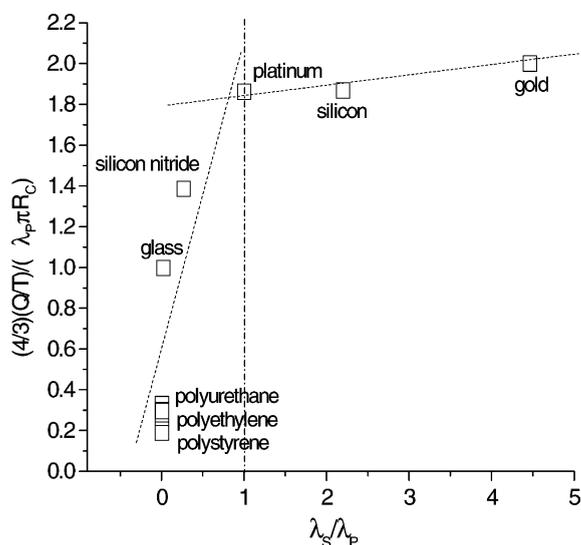
Fig. 4. The variation of the reduced heat dissipation during the physical contact vs. the thermal conductivity of various materials reduced to dimensionless units according to the Eq. (5). Separation between low and high conductive materials is defined by the thermal conductivity of the thermal probe (vertical line).

responsible for heat dissipation at the contact point is directly proportional to the surface thermal conductivity of the materials tested, or $\lambda \sim \lambda_S$. Contrary, for high thermally conductive materials with thermal conductivity higher than that of platinum, a thermal sink is represented by the surface and the thermal tip becomes the poorly conductive counterpart. In this case, the Eq. (4) predicts a virtually constant composite thermal conductivity, $\lambda \cong \lambda_P$, with essentially no regard to the actual material tested. Therefore, a virtually constant value of measured heat dissipation should be anticipated for highly conductive materials. This consideration explains reasonably well the observed trend, but requires further testing for a wider variety of materials with thermal conductivities higher than that of platinum in lieu of the limited number of materials with high thermal conductivity tested here. Finally, we can conclude that from a practical point of view, for a wide variety of materials excluding high thermally conductive metals, the linear relationship between the measured heat dissipation and the bulk thermal conductivity holds with fair accuracy.

We analyzed the heating rate dependence on the melting temperature as evaluated independently from DSC and μTA measurements (see examples of data

analysis in Fig. 5). We recorded DSC runs for several polymer materials in a wide range of heating rates from 10 to 500 °C min$^{-1}$. As expected, DSC-measured melting temperatures shifted to higher values with increasing heating rate (see data for PET in Fig. 6) [23,24]. A very similar trend was observed for μTA measurements although at a higher range of heating rates, from 60 to 1500 °C min$^{-1}$ (Fig. 6). Very different slopes obtained from different measurements are apparently caused by the very different nature of the heat dissipation in a calorimetric cell and in the tip/ surface contact area. However, the extrapolation to zero heating rate, in order to obtain the "equilibrium" melting temperature, produced very similar results for both techniques (257 ± 1 °C) (Fig. 6).

Because the probe heat dissipation critically depends upon the probe/surface contact area, we analyzed the mechanical contribution in the microthermal response signal. We used a PS sample with 5 mm thickness and TMA instrumentation to obtain the temperature variation of the Young's modulus. The cylindrical probe with a diameter of 6.95 mm was subjected to an applied force of 100 mN and a heating rate of 30 °C min$^{-1}$. From the variation of indenter position, we estimated the probe penetration and the temperature dependence of Young's modulus by using the equation for "the cylinder–plane" system (Fig. 7) [25]. As expected, the elastic modulus decreased by three orders of magnitude in the vicinity of the glass transition temperature. Using the Eq. (3) and the Hertzian model for the probe–surface contact [19–21], we estimated the temperature variation of heat dissipation in the form:

$$Q_T = Q_0 \frac{\lambda_T}{\lambda_0} \sqrt[3]{\frac{E_T}{E_0}} \frac{T}{T_0}, \quad (W) \qquad (6)$$

where $Q_0$ is the heat dissipation at the initial (room) temperature, $T$ the current probe temperature and $T_0$ the initial (room) probe temperature; $E_T$ is the Young's modulus variation versus probe temperature as revealed by TMA measurements, $E_0$ is the Young's modulus at room temperature, $\lambda_T$ and $\lambda_0$ are the thermal conductivities at current and room temperatures, respectively.

Fig. 7 represents the results simulated with Eq. (6) by using the TMA experimental data for elastic modulus values. Simulated heat dissipation, associated solely with an increasing physical contact area due
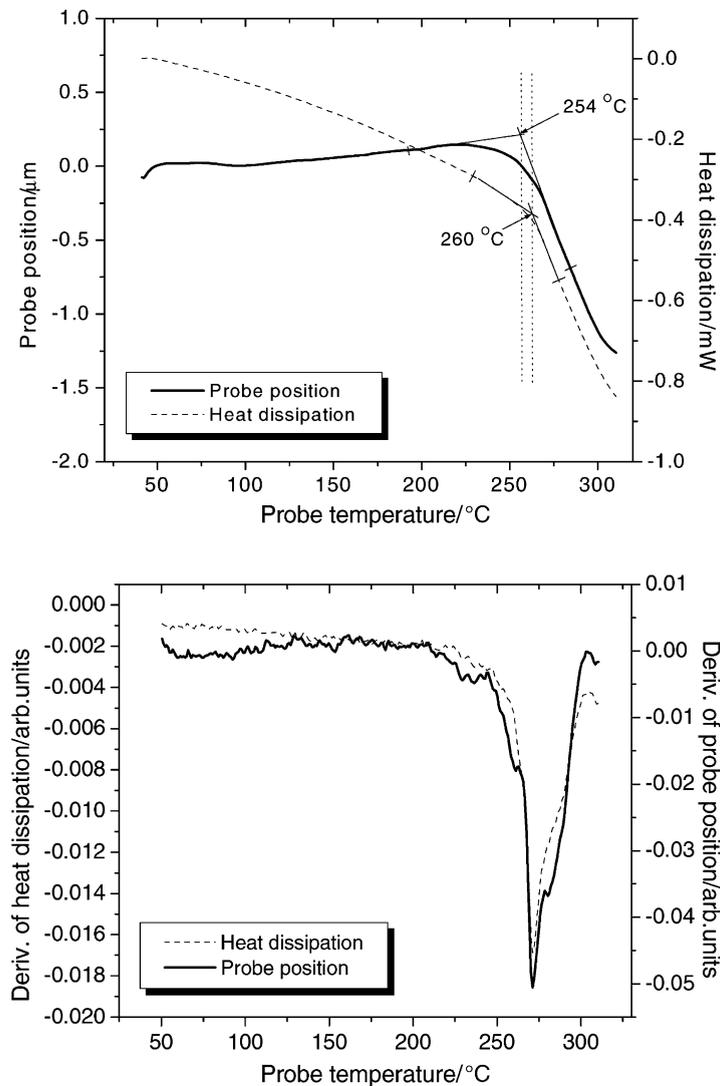
Fig. 5. Microthermal probing of PET bulk sample that demonstrates the difference in the measured melting temperature from two different signals: onset of heat dissipation and probe vertical position (top), and their derivatives (bottom). The heating rate is 10 °C s⁻¹.

to increasing indentation depth (thermomechanical behavior), showed a dramatic increase in the temperature range above glass transition. Experimentally observed increase in the heat dissipation for the μTA experiment was, in fact, similar to the simulated response, but the absolute scale of the variation was smaller. Considering the fact that the thermal conductivity of glassy polymers varies modestly with temperature (within 10%) [23], we can conclude that a variation of heat dissipation as measured by μTA

was caused by the variation of the physical contact area as a result of the gradual "sinking" of the thermal probe into the compliant material. Obviously, the variation of heat dissipation is affected by additional factors, which remain unaccounted for by a simple mechanistic model. The role of these additional factors (e.g. different mechanisms of heat transfer, interplay between heat dissipation and its diffusion from the contact area) should be a subject of further investigations.
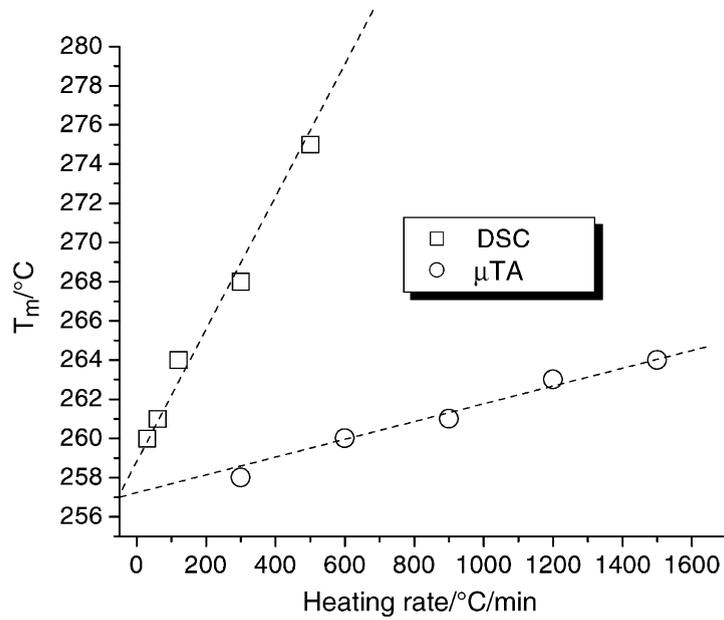
Fig. 6. Heating rate dependence on the melting temperature of polyethyleneterephtalate (PET) measured independently with DSC and µTA techniques.
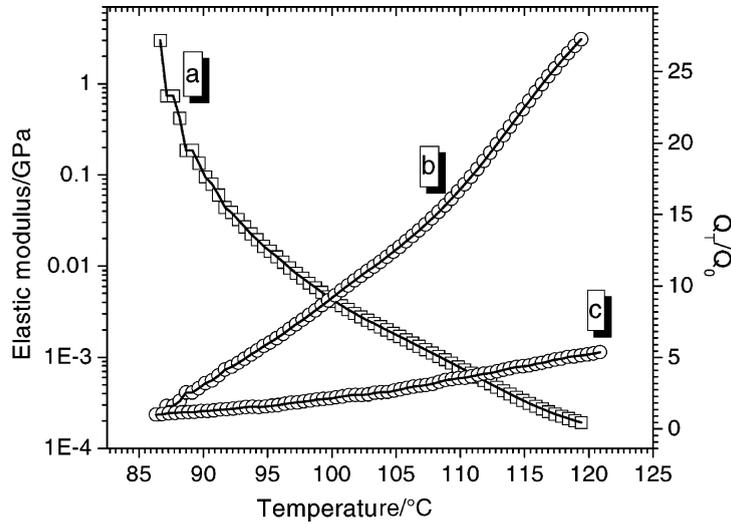


Fig. 7. The temperature dependence of Young's modulus obtained from TMA measurements for PS (a); simulated heat dissipation produced by a "sinking" tip (b) and heat dissipation measured by µTA (c).

## Acknowledgements

## References

[1] C.C. Williams, H.K. Wickramasinghe, Photoacoustic and Photothermal Phenomena, Springer, Berlin, 1988, p. 364.

 [2]  A. Majumdar, J.P. Carrejo, J. Lai, J. Appl. Phys. Lett. 62 (1993) 2501.
 [3]  A. Hammiche, M. Reading, H.M. Pollock, M. Song, D.J. Hourston, Rev. Sci. Instrum. 67 (12) (1996) 4268.
 [4]  A. Hammiche, H.M. Pollock, M. Song, D. Hourston, J. Meas. Sci. Technol. 7 (1996) 142.
 [5]  A. Hammiche, D.J. Hourston, H.M. Pollock, M. Reading, M. Song, J. Vac. Sci. Technol. 14 (1996) 1486.
 [6]  A. Hammiche, H.M. Pollock, M. Reading, M. Clayborn, P.H. Turner, K. Jewkes, Appl. Spectros. 53 (1999) 810.
 [7]  V.V. Gorbunov, N. Fuchigami, J.L. Hazel, V.V. Tsukruk, Langmuir 15 (1999) 8340.
 [8]  V.V. Gorbunov, N. Fuchigami, V.V. Tsukruk, Probe Micros. 2 (2000) 53.
 [9]  V.V. Gorbunov, N. Fuchigami, V.V. Tsukruk, Probe Micros. 2 (2000) 65.
[10]  H.M. Pollock, A. Hammiche, M. Song, D.J. Hourston, M. Reading, J. Adhesion 67 (1998) 217.
[11]  V.V. Gorbunov, N. Fuchigami, V.V. Tsukruk, High Performance Polym. 12 (2000) 603.
[12]  F. Depasse, S. Gomes, N. Trannoy, P. Grossel, J. Phys. D: Appl. Phys. 30 (1997) 3279.
[13]  M. Song, D.J. Hourston, M. Reading, H.M. Pollock, A. Hammiche, J. Therm. Anal. Calorim. 56 (3) (1999) 991.
[14]  H. Block, in: Proceedings of the General Discussion on Lubrication and Lubricants, Inst. Mech. Eng. 2 (1937) 222.
[15]  J.C. Jaeger, Proc. R. Soc. 76 (Part III) (1942) 22.
[16]  V.V. Haritonov, N.V. Yakutin, Tech. Phys. J. 67 (2) (1997) 1.
[17]  J.J. Salgon, F. Robbe-Valloire, J. Blouet, J. Bransier, Int. J. Heat Mass Transfer 40 (5) (1997) 1121.
[18]  K.L. Johnson, in: V.V. Tsukruk, K.J. Wahl (Eds.), Microstructure and Microtribology of Polymer Surfaces, American Chemical Society, Vol. 741, Washington, DC, 2000, p. 24.
[19]  N. Burnham, D. Dawn, R. Mowery, R. Colton, Phys. Rev. Lett. 64 (16) (1990) 1931.
[20]  S.A. Chizhik, Z. Huang, V.V. Gorbunov, N.K. Myshkin, V.V. Tsukruk, Langmuir 14 (10) (1998) 2606.
[21]  V.V. Tsukruk, K. Wahl (Eds.), Microstructure and Microtribology of Polymer Surfaces, ACS Symposium Series, Vol. 741, Washington, DC, 2000.
[22]  V.V. Tsukruk, Z. Huang, S.A. Chizhik, V.V. Gorbunov, J. Mater. Sci. 33 (1998) 4905.
[23]  D.W. Van Krevelen, Properties of Polymers, Elsevier, Amsterdam, 1997.
[24]  B. Wunderlich, Thermal Analysis, Academic Press, New York, 1990.
[25]  A.I. Sviridenok, S.A. Chizhik, M.I. Petrokovets, Mechanics of a Discreet Friction Contact, Nauka I Tekhnika, Minsk, 1990.